Extended Abstract, 28th Conf. on Severe Local Storms
Amer. Meteor. Soc., Portland, OR, November 7-11, 2016

12B.4 ASSIMILATION OF Z_{DR} COLUMNS FOR IMPROVING MODEL SPIN-UP

Jacob Carlin[1,3], Jidong Gao[2], Jeffrey Snyder[1], Alexander Ryzhkov[1]
[1]*Cooperative Institute for Mesoscale Meteorological Studies, Norman, Oklahoma*
[2]*National Severe Storms Laboratory, NOAA, Norman, Oklahoma*
[3]*School of Meteorology, University of Oklahoma, Norman, Oklahoma*

1. INTRODUCTION

Over the past few decades, the development of convection-resolving models has necessitated the need for observations to aid in reducing model spin-up time. Radar has proven essential in this regard, as it is one of the only sources of data available of sufficient temporal and spatial resolution to resolve convective features on scales comparable to the models. As such, the assimilation of radar data has remained a prominent research focus, particularly as the community moves toward operational implementation of convection-resolving models in the warning decision process with the help of initiating NOAA's Warn-on-Forecast project (Stensrud 2009, 2013).

Many methods of radar data assimilation have been explored. One of the most simple and straightforward methods is through the use of a so-called "cloud analysis" scheme (Zhang et al. 1998; Zhang 1999; Brewster 2002; Hu et al. 2006). Cloud analysis schemes assimilate radar data indirectly by using semi-empirical equations to adjust the model hydrometeor mixing ratios, humidity, and temperature field from reflectivity Z. While the use of cloud analysis schemes have shown positive impacts in reducing model spin-up time and improving short term forecasts (e.g., Hu et al. 2006; Xue et al. 2014), a number of arbitrary parameters are used to update the aforementioned state variables from Z.

Dual-polarization radars transmit and receive both horizontally and polarized electromagnetic waves, from which more information about a target's size, shape, orientation, and composition can be garnered than from Z alone. Dual-polarization data has been successfully leveraged for many applications including quantitative precipitation estimation (e.g., Ryzhkov et al. 2005), hydrometeor classification (e.g., Park et al. 2009), hail identification (e.g., Heinselman and Ryzhkov 2006), and hail size discrimination (e.g., Ryzhkov et al. 2013a,b). In addition to these applications, dual-polarization radar has also led to the discovery of many distinct signatures in convection, such as Z_{DR} columns.

Z_{DR} columns are tall, narrow protrusions of enhanced Z_{DR} above the environmental 0˚C level caused by large, oblate raindrops and wet ice particles being lofted by the updraft and undergoing time-dependent freezing (e.g., Kumjian et al. 2014). Because they are caused by lofting of particles by the updraft, Z_{DR} columns can be used as a proxy for updraft location. More recently, work by Picca et al. (2010) and Kumjian et al. (2014) has shown strong correlations between Z_{DR} column height and updraft intensity and surface hail content.

Despite the benefits dual-polarization radar offers for retrieving microphysical information, little work has focused on directly assimilating actual dual-polarization observations. The majority of studies that incorporate dual-polarization data either assimilate simulated observations (e.g., Jung et al. 2008a,b) or use simulated dual-polarization variables from model runs to compare to observations as a form of model validation (e.g., Johnson 2016). Because of deficiencies in convective scale NWP models' microphysical processes, the direct assimilation of dual-polarization data for real data cases is still not mature (Posselt 2015). This study aims to assimilate dual-polarization observations of Z_{DR} columns through a modified cloud analysis routine.

2. DESCRIPTION OF MODIFIED CLOUD ANALYSIS

The modified cloud analysis retains much of its formulation from the original ADAS Cloud Analysis (Zhang et al. 1998; Zhang 1999; Brewster 2002; Hu et al. 2006). Radar data are processed, quality controlled, and mosaicked to the model grid. Clouds are inserted anywhere Z exceeds a threshold (with a default threshold of 15 dBZ used). Cloud water and ice is added according to the Smith-Feddes model (Haines et al. 1989) with a reduction for entrainment. Hydrometeor mixing ratios are estimated from Z using simple semi-empirical equations from Smith et al. (1975) and Lin et al. (1983). A temperature adjustment to account for latent heat release is then performed, which can be calculated by user choice either ac-

Corresponding author address: Jacob Carlin, Cooperative Institute for Mesoscale Meteorological Studies, 120 David Boren Blvd, Norman OK 73072.
Email: jacob.carlin@noaa.gov.

cording to the added cloud water and ice innovations or by using moist-adiabatic parcel ascent from cloud base. The moisture field is then re-adjusted to ensure saturation in updrafts.

Tong (2015) found that saturating based on Z results in too much moisture being added and large degradations in forecast skill. Tong (2015) proposed a method for estimating water vapor from vertical velocity with positive impacts noted, but the method relies on a tenuous q_v-w relationship and necessitates accurate downdraft speeds. Additionally, the location and magnitude of the added temperature perturbations strongly affect the development of updrafts and the convective circulations within the model.

The present study proposes a new method to utilize Z_{DR} columns to localize the temperature and moisture increments added to the model. Vertical cross sections of relative humidity, latent heating rate, Z_{DR}, and Z from the Hebrew University Cloud Model (HUCM; Khain et al. 2004) and coupled polarimetric operator (Rhyzkov et al. 2011) at S-band are shown in Figure 1. The HUCM is a two-dimensional, non-hydrostatic spectral bin cloud model. Figure 1 shows that plumes of saturation and latent heat release are located within and above Z_{DR} columns. However, it is also clear from Figure 1 that saturating everywhere $Z \geq 15$ dBZ would result in too much moisture being added to the system. Based on these results, the use of Z_{DR} columns to localize the temperature and moisture increments appears to be well justified.

The method for detecting Z_{DR} columns is similar to that of Snyder et al. (2015). Areas with $Z \geq 10$ dBZ and $\rho_{hv} \geq 0.85$ are searched for model columns that contain two or more vertically contiguous grid cells with $Z_{DR} \geq 1.0$ above the 0˚C level but below the -20˚C level to prevent contamination from oblate ice crystals. Once Z_{DR} column grid cells are identified, the model column containing those grid cells is warmed and saturated as described previously. Heat is also added to one grid box in each direction outside of the detected column to prevent mixing out in the case of narrow columns, and moisture is added to additional grid boxes in each direction proportional to the detected height of the Z_{DR} columns. In addition, a simple drying procedure is added that dries each grid cell by half of the difference between that cell's relative humidity and 100% relative humidity if the cell has a relative humidity ≥ 80% with no detected Z_{DR} column. Figure 2 shows a comparison of the posterior analysis of 2-km relative humidity for the original ('CONTROL') and modified ('ZDRCOL') methods as an example demonstrating the impact of these changes. Compared to CONTROL, ZDRCOL features a smaller area of saturation in the primary storm that is further to the southwest. Additionally, the weakening storm to the north is not significantly saturated in the ZDRCOL run, while a developing storm further to the south is saturated while it is not in the CONTROL run.

3. EXPERIMENTAL DESIGN

The Advanced Regional Prediction System (ARPS; e.g., Xue et al. 2001) and its 3DVAR data assimilation system (Gao et al. 2004) were used for this study. Parameterization schemes used include Milbrandt-Yau double moment microphysics (Milbrandt and Yau 2005a,b), a 1.5-order TKE turbulence closure scheme, the planetary boundary layer parameterization of Sun and Chang (1986), the NASA Goddard scheme for shortwave and longwave radiation (Chou 1990, 1992), and a two-layer force-store soil model from Noilhan and Planton (1989). A one-way nest was used with an outer domain of 1200 x 1200 km with 4-km grid spacing and an inner domain of 500 x 500 km with a 1-km grid spacing. Both nests contained 53 stretched vertical levels. The initial background was provided by the North American Mesoscale model and was integrated forward to provide lateral boundary conditions for the inner nest. A 1-hr spin-up period was performed on the outer nest, interpolated to the inner nest, and used to launch another 1-hr spin-up on the inner nest. This was then used as the initial background for all subsequent experiments.

The 19 May 2013 central Oklahoma tornado outbreak is examined in this study. This outbreak resulted in 8 tornadoes, including an EF4 that struck Shawnee, Oklahoma responsible for 2 deaths and 14 injuries. Unless otherwise noted, radar data from the Twin Lakes, OK WSR-88D radar (KTLX) are used. Beginning at 20:00 UTC, radial velocity and surface observations from the Oklahoma Mesonet are assimilated using the ARPS 3DVAR program (Gao et al. 2004), and dual-polarization data are assimilated using the cloud analysis every 10 minutes. Every 30 minutes, a 1-hr forecast is launched, with the final forecast launched at 23:00 UTC. The assimilation procedure is depicted graphically in Figure 3. In addition to the two aforementioned primary runs ('Control' and 'ZDRCOL'), three additional runs were performed: 'Control_AllRad' which uses the traditional cloud analysis but incorporates radar data from four additional sites, 'ZDRCOL_NoVr' which uses the modified cloud analysis but excludes radial velocity, and 'ZDRCOL_LHRH', which modifies *only* the moisture and temperature field using the

modified cloud analysis while excluding cloud and precipitation hydrometeors. These extra runs were performed as sensitivity tests as the primary focus is on the Control and ZDRCOL runs.

4. PRELIMINARY RESULTS

A composite of maximum updraft swaths at each analysis time is shown in Figure 4 for the Control and ZDRCOL runs. This composite spans 20:00 – 23:00 UTC, which covers the initial generation of convection through the start of the EF4 tornado in eastern Cleveland County (in the center of the domain). The control run features a noisy field with many potentially spurious updrafts, along with a pronounced northward bias of storm propagation compared to the observed tornado tracks, as seen in other studies examining this case (e.g., Wheatley et al. 2015). In contrast, the ZDRCOL run features much more consolidated and consistent updraft tracks. The $w_{max} \geq 30$ m s^{-1} contour is generally larger in the ZDRCOL run. Additionally, the northward bias of storm propagation is much less pronounced, with the northern storm following the observed tornado track very well and the southern storm featuring a lesser northward bias.

The accumulated forecast 1-6 km updraft helicity (UH) swaths for three different forecast times are shown in Figures 5-7. During the first launched forecast at 20:30 UTC (Fig. 5), both Control and ZDRCOL feature a storm track that is too far to the north. However, the ZDRCOL UH swath is more consolidated and has a smaller bias in the northward component of motion compared to the Control run. The ZDRCOL run is also a bit slower (closer to the truth), with the center of the UH swath moving approximately 10 km less in the period than the Control run. The improvements over Control are most evident in the forecast launched at 21:30 UTC (Fig. 6), approximately 10 minutes before the start of the northern EF3 tornado. The Control run features multiple UH swaths. There is no identifiable strong UH swath associated with the northern EF3 tornado (tornado 'C' in Fig. 2) ongoing at this time, with UH swaths too far to the northeast. There are also multiple UH swaths associated with a weaker non-tornadic supercell that passed in between the two long-tracked tornadoes. In sharp contrast, the ZDRCOL run captures the UH swath of the northern tornado very well, with only a slight bias in forward speed. It correctly captures a weaker UH swath associated with the middle supercell. Finally, it has the additional advantage of capturing the developing southern supercell at an earlier stage (eventually associated with tornado 'D' in Fig. 2), which was completely absent in the forecast for the Control launched at 21:30 UTC. Finally, the launched forecast an hour later at 22:30 UTC (Fig. 7) shows many of the same advantages, with the ZDRCOL run now featuring a strong, consolidated UH swath associated with the southern tornado (tornado 'D') and a much noisier, less coherent appearance in the Control run.

To further examine the improvements seen in the 21:30 UTC UH swath forecast, the 1-km Z for the Control and ZDRCOL runs is compared to the observed 1-km Z in Figure 8 in 10 min increments starting at 21:40 UTC. The model Z was computed using the T-matrix based code of Jung et al. (2010). As described above, it is clear that the Control run features a strong northward and forward speed bias compared to observations. The middle supercell fails to remain distinct, and by 22:20 UTC unrealistic banding features are observed in the Z. The storms are larger than those observed with large expanses of $Z \geq 45$ dBZ. In contrast, the ZDRCOL run is much closer to the observations. The forecast storms are closer in size and position to the observed storms, with three distinct supercells featuring identifiable hooks still present 1-hr into the forecast at 22:30 UTC.

Based on these encouraging qualitative results, the equitable threat score (ETS) was computed for the composite reflectivity at 20, 30, and 40 dBZ thresholds for each launched forecast, where higher values indicate better agreement with the observed Z. ZDRCOL exhibits a notable improvement over Control for the 30 and 40 dBZ thresholds through the entire duration of each forecast. Little improvement is seen for the 20 dBZ threshold. The additional sensitivity runs are also compared here. Both the ZDRCOL_NoVr and ZDRCOL_LH runs outperform the Control run, highlighting the dominant effect on the resulting forecast the latent heat and moisture adjustments based on dual-polarization data have. Note that the ZDRCOL_LH ETS is initially low as the hydrometeor field used to compute Z is not updated, resulting in the initial model Z not matching the observed Z as done in the other runs. At 30 and 40 dBZ thresholds, the ZDRCOL run even outperforms the Control_AllRad, again speaking to the importance of the temperature and moisture increments assimilated into the model.

5. SUMMARY AND FUTURE WORK

A novel method of assimilating Z_{DR} columns is presented via a modification of an existing cloud analysis. Changes are made to localize positive temperature and moisture increments where Z_{DR}

columns are detected. This new method was applied to the 19 May 2013 tornado outbreak in central Oklahoma. Notable improvements were seen over the traditional cloud analysis, including more consolidated updraft tracks, smaller errors in position and storm motion, longer lead time on nascent convection, and an improved quantitative measure (i.e., ETS) for moderate values of *Z*.

This study represents an initial *proof of concept* investigation of assimilating dual-polarization radar data using the simple and efficient cloud analysis method. Despite these encouraging preliminary results, much work remains to be done. First, more cases need to be analyzed to obtain a broader perspective about the method's utility. The case selected here featured very prominent, long-lived Z_{DR} columns with good radar coverage, but the performance of the method in less canonical cases should be evaluated. Testing of various microphysics schemes should also be done to study the sensitivity of the method to the microphysics scheme chosen. The details of both the Z_{DR} column detection criteria and the application of the temperature and moisture increments (e.g., cycling frequency, nudging of increments, assimilating increments variationally instead of the direct insertion used here) should be further scrutinized and tested. Finally, more quantitative verification metrics and testing the impact of assimilating various combinations of data needs to be performed.

Acknowledgments: This research was supported by NSF Grant AGS-1341878. The computing for this project was performed at the OU Supercomputing Center for Education & Research (OSCER) at the University of Oklahoma (OU). The authors would also like to thank Jessica Erlingis and Elizabeth Smith for reviewing this manuscript.

REFERENCES

Brewster, K., 2002: Recent advances in the diabatic initialization of a non-hydrostatic numerical model. *15th Conf. on Numerical Weather Prediction/21st Conf. on Severe Local Storms*, San Antonio, TX, Amer. Meteor. Soc., J6.3.

Chou, M.-D., 1990: Parameterizations for the absorption of solar radiation by O_2 and CO_2 with application to climate studies. *J. Climate*, **3**, 209-217.

Chou, M.-D., 1992: A solar radiation model for use in climate studies. *J. Atmos. Sci.,* **49**, 762-772.

Fierro, A. O., E. R. Mansell, C. L. Ziegler, and D. R. MacGorman, 2012: Application of a lightning data assimilation technique in the WRF-ARW model at cloud-resolving scales for the tornado outbreak of 24 May 2011. *Mon. Wea. Rev.,* **140**, 2609-2627.

Fierro, A. O., J. Gao, C. L. Ziegler, E. R. Mansell, D. R. MacGorman, and S. R. Dembek, 2014: Evaluation of a cloud-scale lightning data assimilation technique and a 3DVAR method for the analysis and short-term forecast of the 29 June 2012 derecho event. *Mon. Wea. Rev.,* **142**, 183-202.

Gao, J., M. Xue, K. Brewster, and K. K. Droegemeier, 2004: A three-dimensional variational data analysis method with recursive filter for Doppler radars. *J. Atmos. Oceanic Technol.,* **21**, 457-469.

Haines, P. A., J. K. Luers, and C. A. Cerbus, 1989: The role of the Smith-Feddes model in improving the forecasting of aircraft icing. *3rd Conf. on the Aviation Weather System*, Anaheim, CA, Amer. Meteor. Soc., 258-263.

Heinselman, P. L., and A. V. Ryzhkov, 2006: Validation of polarimetric hail detection. *Wea. Forecasting*, **21**, 839-850, doi:101175/WAF956.1.

Hu, M., M. Xue, and K. Brewster, 2006: 3DVAR and cloud analysis with WSR-88D level-II data for the prediction of the Fort Worth, Texas tornadic thunderstorms. Part I: Cloud analysis and its impact. *Mon. Wea. Rev.,* **134**, 675-698.

Johnson, M., Y. Jung, D. Dawson, and M. Xue, 2016: Comparison of simulated polarimetric signatures in idealized supercell storms using two-moment bulk microphysics schemes in WRF. *Mon. Wea. Rev.,* **144**, 971-996.

Jung, Y., G. Zhang, and M. Xue, 2008a: Assimilation of simulated polarimetric radar data for a convective storm using the ensemble Kalman filter. Part I: Observation operators for reflectivity and polarimetric variables. *Mon. Wea. Rev.,* **136**, 2228-2245.

Jung, Y., G. Zhang, M. Xue, and J. M. Straka, 2008b: Assimilation of simulated polarimetric radar data for a convective storm using the ensemble Kalman filter. Part II: Impact of polarimetric data on storm analysis. *Mon. Wea.*

Rev., **136**, 2246-2260.

Jung, Y., M. Xue., and G. Zhang, 2010: Simulations of polarimetric radar signatures of a supercell storm using a two-moment bulk microphysics scheme. *J. Appl. Meteor. Climatol.,* **49**, 146-163.

Khain, A., A. Pokrovsky, M. Pinsky, A. Seifert, and V. Phillips, 2004: Simulation of effects of atmospheric aerosols on deep turbulent convective clouds using a spectral microphysics mixed-phase cumulus cloud model. Part I: Model description and possible applications. *J. Atmos. Sci..,* **61**, 2963-2982.

Kumjian, M. R., A. P. Khain, N. Benmoshe, E. Ilotoviz, A. V. Ryzhkov, and V. T. Phillips, 2014: The anatomy and physics of ZDR columns: Investigating a polarimetric radar signature with a spectral bin microphysical model. *J. Appl. Meteor. Climatol.,* **53**, 1820-1843.

Lin, Y.-L., R. D. Farley, and H. D. Orville, 1983: Bulk parameterization of the snow field in a cloud model. *J. Climate Appl. Meteor.,* **22**, 1065-1092.

Milbrandt, J., and M. Yau, 2005a: A multimoment bulk microphysics parameterization. Part I: Analysis of the role of the spectral shape parameter. *J. Atmos. Sci.,* **62**, 3051-3064.

Milbrandt, J., and M. Yau, 2005b: A multimoment bulk microphysics parameterization. Part II: A proposed three-moment closure and scheme description. *J. Atmos. Sci.,* **62**, 3065-3081.

Noilhan, J., and S. Planton, 1989: A simple parameterization of land surface processes for meteorological models. *Mon. Wea. Rev.,* **117**, 536-549.

Park, H., A. V. Ryzhkov, D. S. Zrnić, and K.-E. Kim, 2009: The hydrometeor classification algorithm for the polarimetric WSR-88D: Description and application to an MCS. *Wea. Forecasting,* **24**, 730-748.

Picca, J. C., M. Kumjian, and A. Ryzhkov, 2010: ZDR columns as a predictive tool for hail growth and storm evolution. *25th Conference on Severe Local Storms*, Denver, CO, Amer. Meteor. Soc., 11.3 pp. [Available online at https://ams.confex.com/ams/25SLS/techprogram/paper_175750.htm.].

Posselt, D., X. Li, S. Tushaus, and J. MEcikalski, 2015: Assimilation of dual-polarization radar observations in mixed- and ice-phase regions of convective storms: Information content and forward model errors. *Mon. Wea. Rev.,* **143**, 2611-2636.

Ryzhkov, A. V., S. E. Giangrande, and T. J. Schuur, 2005: Rainfall estimation with a polarimetric prototype of WSR-88D. *J. Appl. Meteor.,* **44**, 502-515.

Ryzhkov, A. V., M. Pinsky, A. Pokrovsky, and A. Khain, 2011: Polarimetric radar observation operator for a cloud model with spectral microphysics. *J. Appl. Meteor. Climatol.,* **50**, 873-894.

Ryzhkov, A. V., M. R. Kumjian, S. M. Ganson, and A. P. Khain, 2013a: Polarimetric radar characteristics of melting hail. Part I: Theoretical simulations using spectral microphysical modeling. *J. Appl. Meteor. Climatol.,* **52**, 2849-2869.

Ryzhkov, A. V., M. R. Kumjian, S. M. Ganson, and P. Zhang, 2013b: Polarimetric radar characteristics of melting hail. Part II: Practical implications. *J. Appl. Meteor. Climatol.,* **52**, 2871-2886.

Smith, P. L., C. G. Myers, and H. D. Orville, 1975: Radar reflectivity factor calculations in numerical cloud models using bulk parameterization of precipitation. *J. Appl. Meteor.,* **14,** 1156-1165.

Snyder, J. C., A. V. Ryzhkov, M. R. Kumjian, A. P. Khain, and J. Picca, 2015: A Z_{DR} column detection algorithm to examine convective storm updrafts. *Wea. Forecasting*, **30**, 1819-1844.

Stensrud, D. J., and Coauthors, 2009: Convective-scale Warn-on-Forecast system: A vision for 2020. *Bull. Amer. Meteor. Soc.,* **90**, 1487-1499.

Stensrud, D. J., and Coauthors, 2013: Progress and challenges with Warn-on-Forecast. *Atmos. Res.,* **123**, 2-16.

Sun, W.-Y., and C.-Z. Chang, 1986: Diffusion model for a convective layer. Part I: Numerical simulation of convective boundary layer. *J. Climate Appl. Meteor.,* **25**, 1445-1453.

Tong, C.-C., 2015: Limitations and potential of complex cloud analysis and its improvement for radar reflectivity data assimilation using OSSEs. PhD dissertation, University of Oklahoma, 174 pp.

Wheatley, D. M., K. H. Knopfmeier, T. A. Jones, and G. J. Creager, 2015: Storm-scale data assimilation and ensemble forecasting with the NSSL Experimental Warn-on-Forecast system. Part I: Radar data experments. *Wea. Forecasting*, **30**, 1795-1817.

Xue., M., K. K. Droegemeier, and V. Wong, 2001: The Advanced Regional Prediction System (ARPS) – a multi-scale nonhydrostatic atmospheric simulation and prediction tool. Part II: Model physics and applications. *Meteor. Atmos. Phys.,* **76**, 143-165.

Xue, M., M. Hue, and A. D. Schenkman, 2014: Numerical prediction of the 8 May 2003 Oklahoma City tornadic supercell and embedded tornado using ARPS with the assimilation of WSR-88D data. *Wea. Forecasting*, **29**, 39-62.

Zhang, J., F. Carr., and K. Brewster, 1998: ADAS cloud analysis. *12th Conf. on Numerical Weather Prediction*, Phoenix, AZ, Amer. Meteor. Soc., 185-188.

Zhang, J., 1999: Moisture and diabatic initialization based on radar and satellite observation. PhD dissertation, University of Oklahoma, 194 pp.

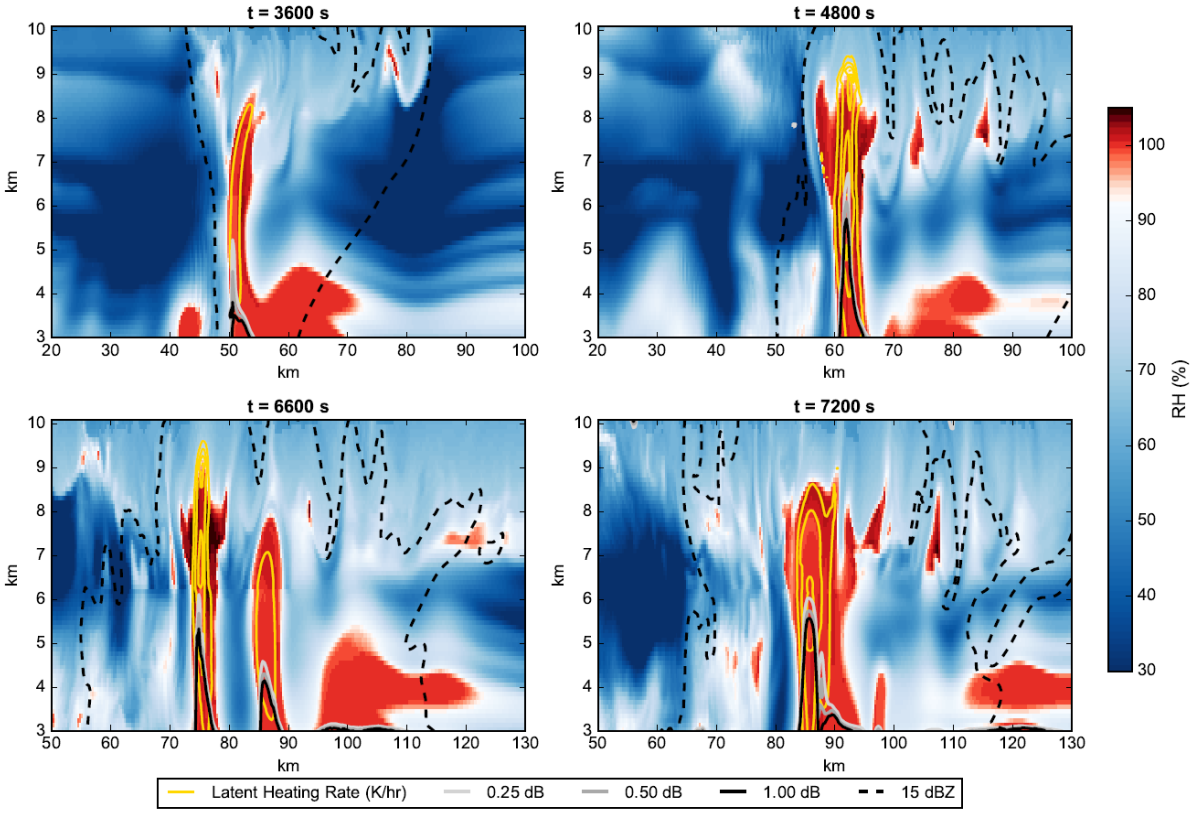

Fig. 1: Vertical cross sections of relative humidity (shading), Z_{DR} (solid gray and black contours), Z (dashed contours), and latent heating rate (solid gold contours in increments of 100 K hr^{-1}) for four different output times from a simulated storm using the HUCM.

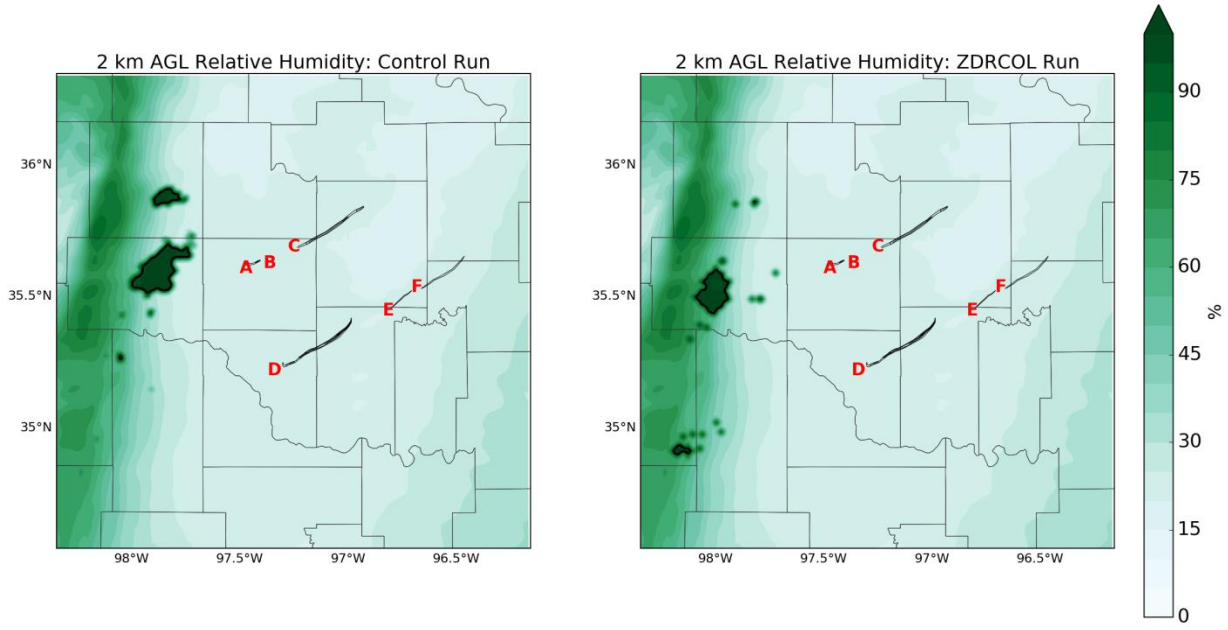

Fig. 2: An example comparison of the posterior 2-km relative humidity (%) at 20:00 UTC after the assimilation of radar data using the (left) traditional cloud analysis and (right) modified cloud analysis. Observed tornado tracks are shown and labeled for the 19 May 2013 tornado outbreak. The solid black contour delineates 95% relative humidity.

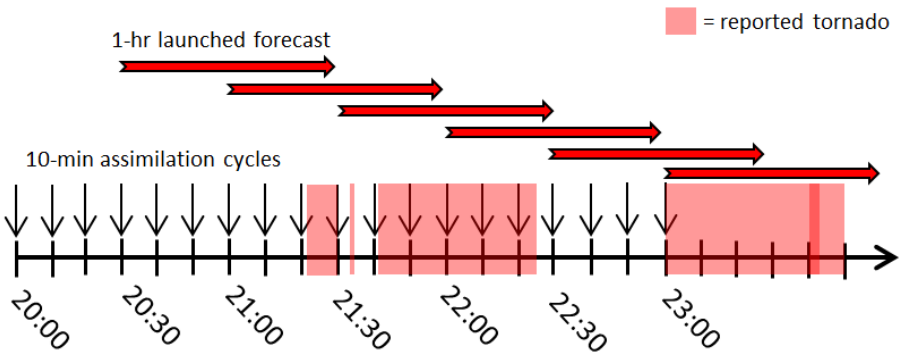

Fig. 3: A diagram showing the cycled assimilation process used. Radar data were assimilated using the cloud analysis every 10 minutes, with 1-hr forecasts launched every 30 minutes beginning at 20:30 UTC. Reported tornado times are shaded. The darker shading at 23:40 UTC represents multiple concurrent tornadoes.

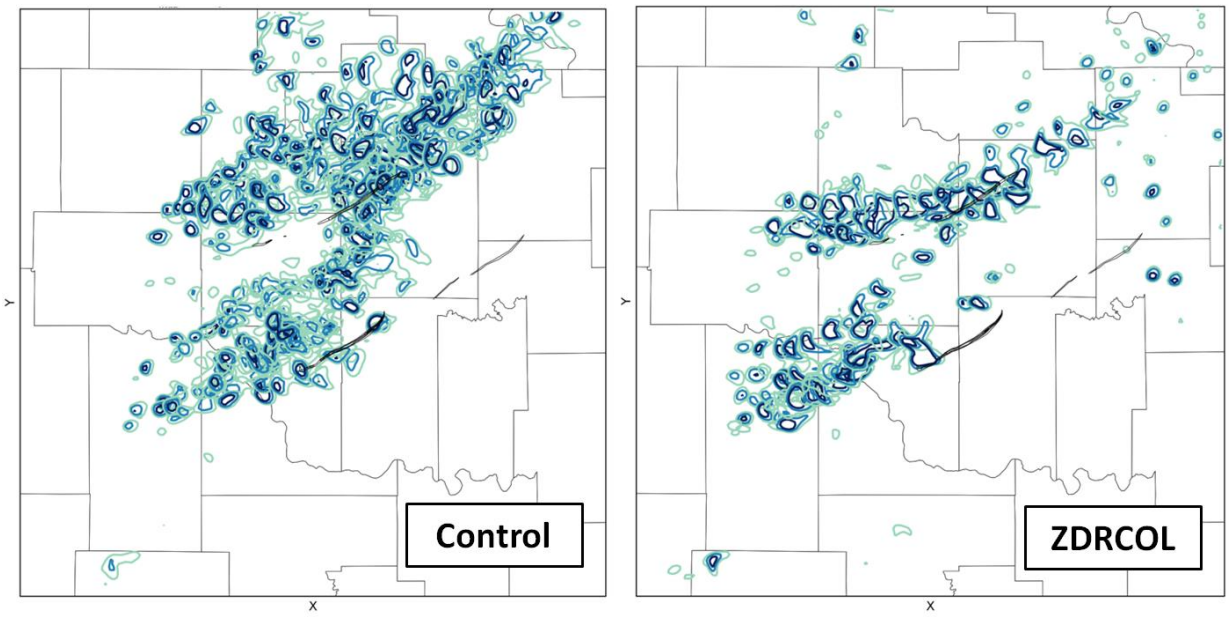

Fig. 4: A composite of the maximum vertical velocity swaths within the column at each analysis time for (left) the traditional cloud analysis and (right) the modified cloud analysis. Contours in teal, light blue, and navy blue indicate 10, 20, and 30 m s^{-1}, respectively.

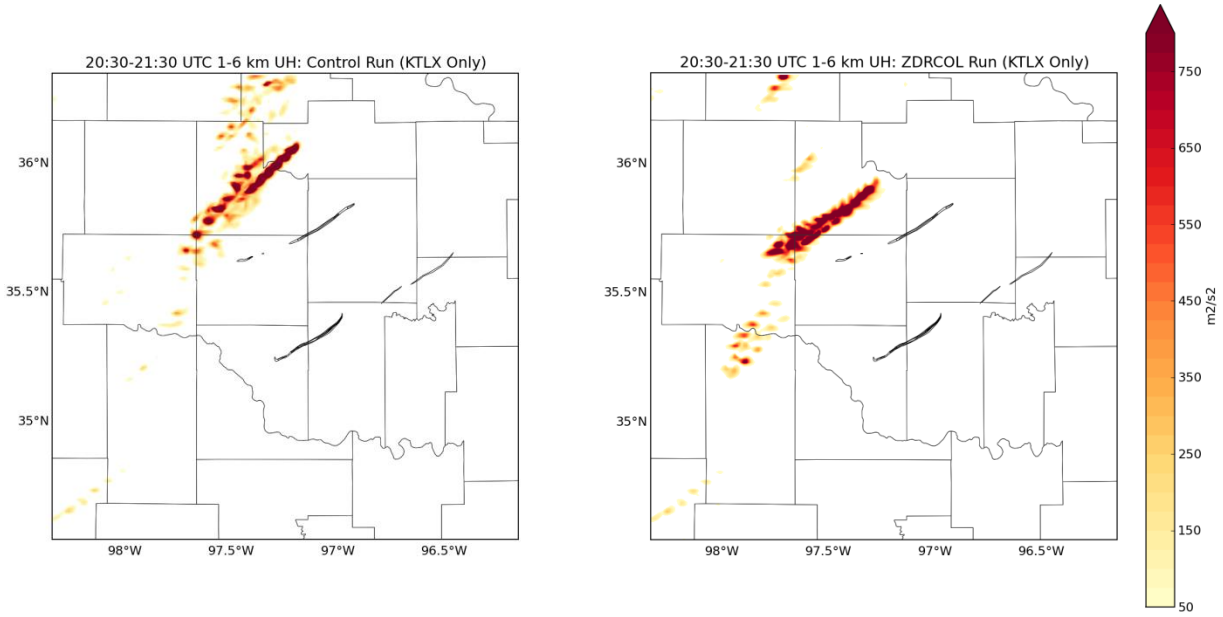

Fig. 5: Accumulated 1-6 km updraft helicity swaths from the 1-hr forecast launched at 20:30 UTC for (left) the traditional cloud analysis and (right) the modified cloud analysis.

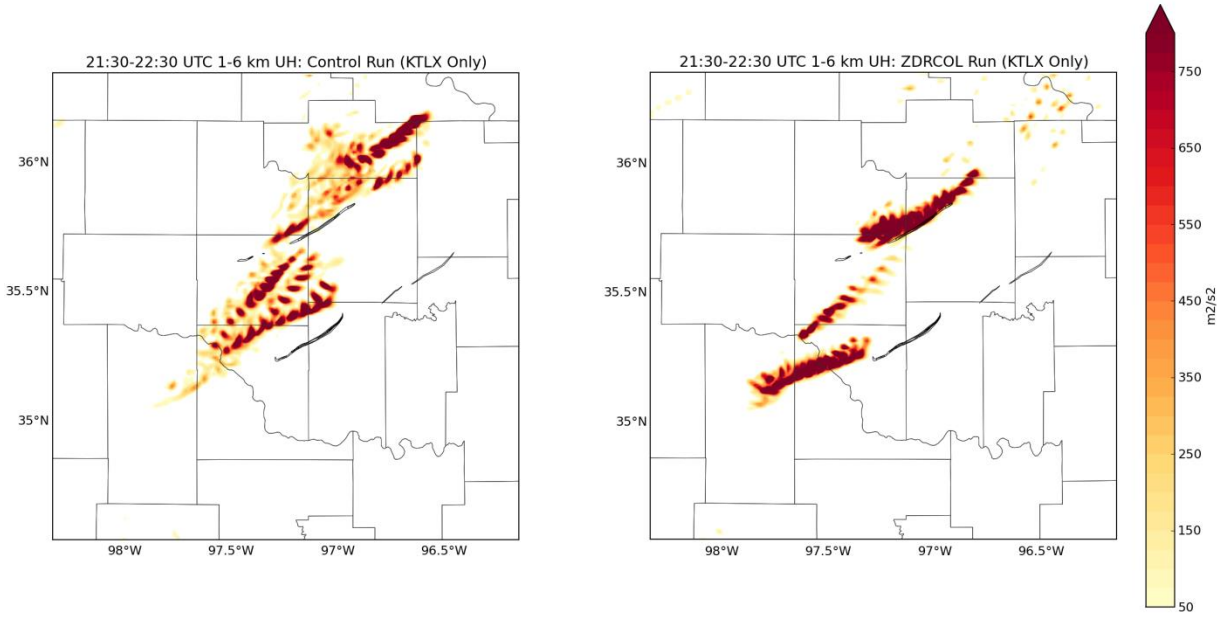

Fig. 6: As in Figure 5, but for the 1-hr forecast launched at 21:30 UTC.

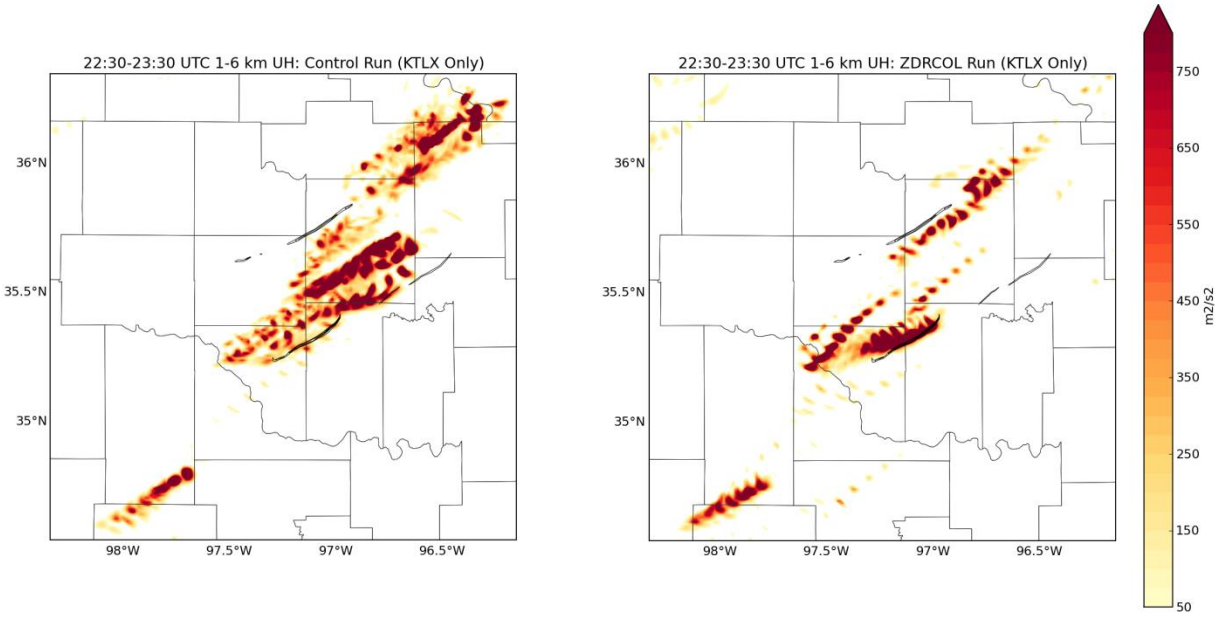

Fig. 7: As in Figure 5, but for the 1-hr forecast launched at 22:30 UTC.

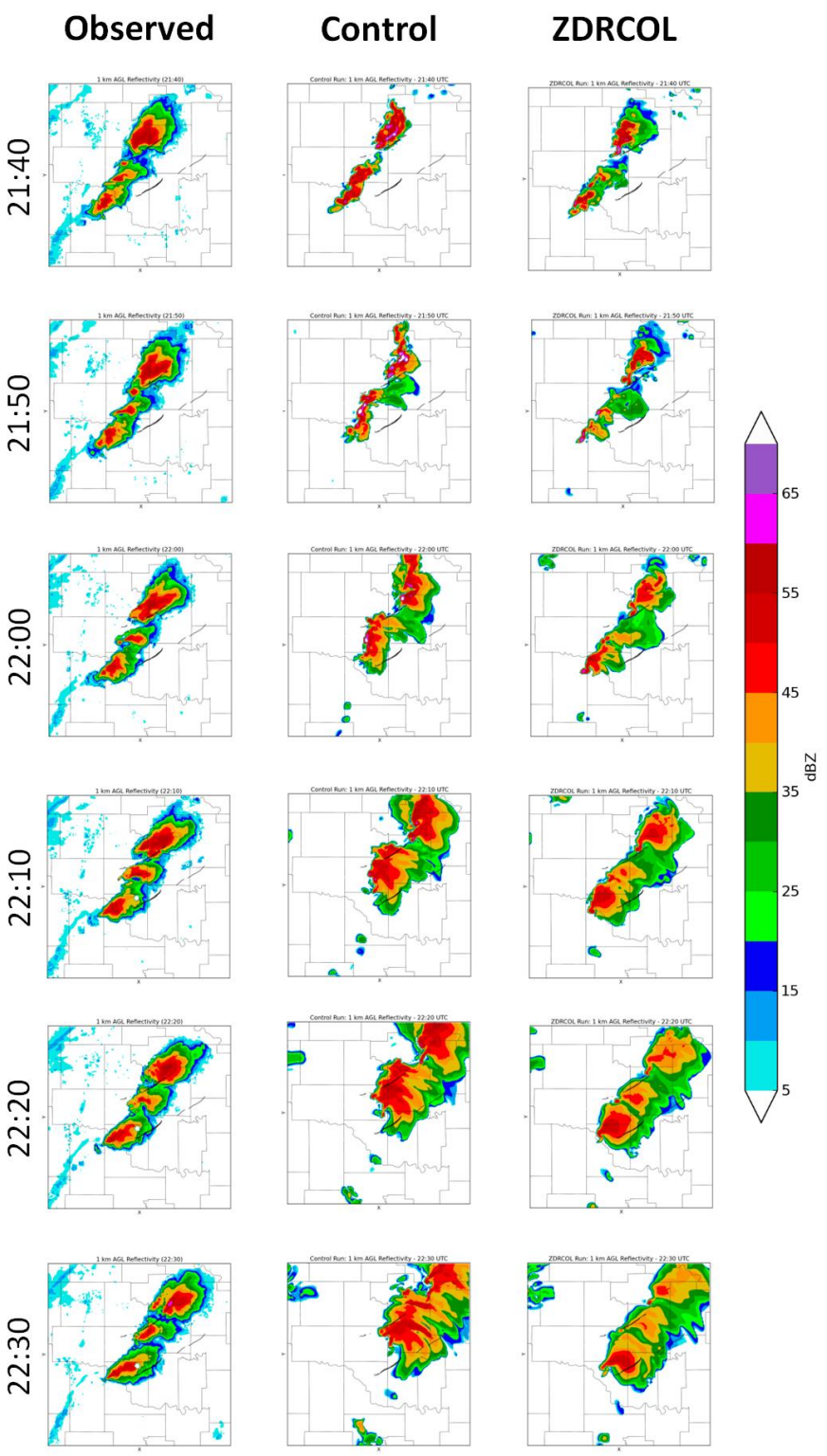

Fig. 8: Comparison of observed tornado tracks and 1-km reflectivity from the (left) observations, (middle) traditional cloud analysis, and (right) modified cloud analysis from the 1-hr forecast launched at 21:30 UTC in 10-min increments.

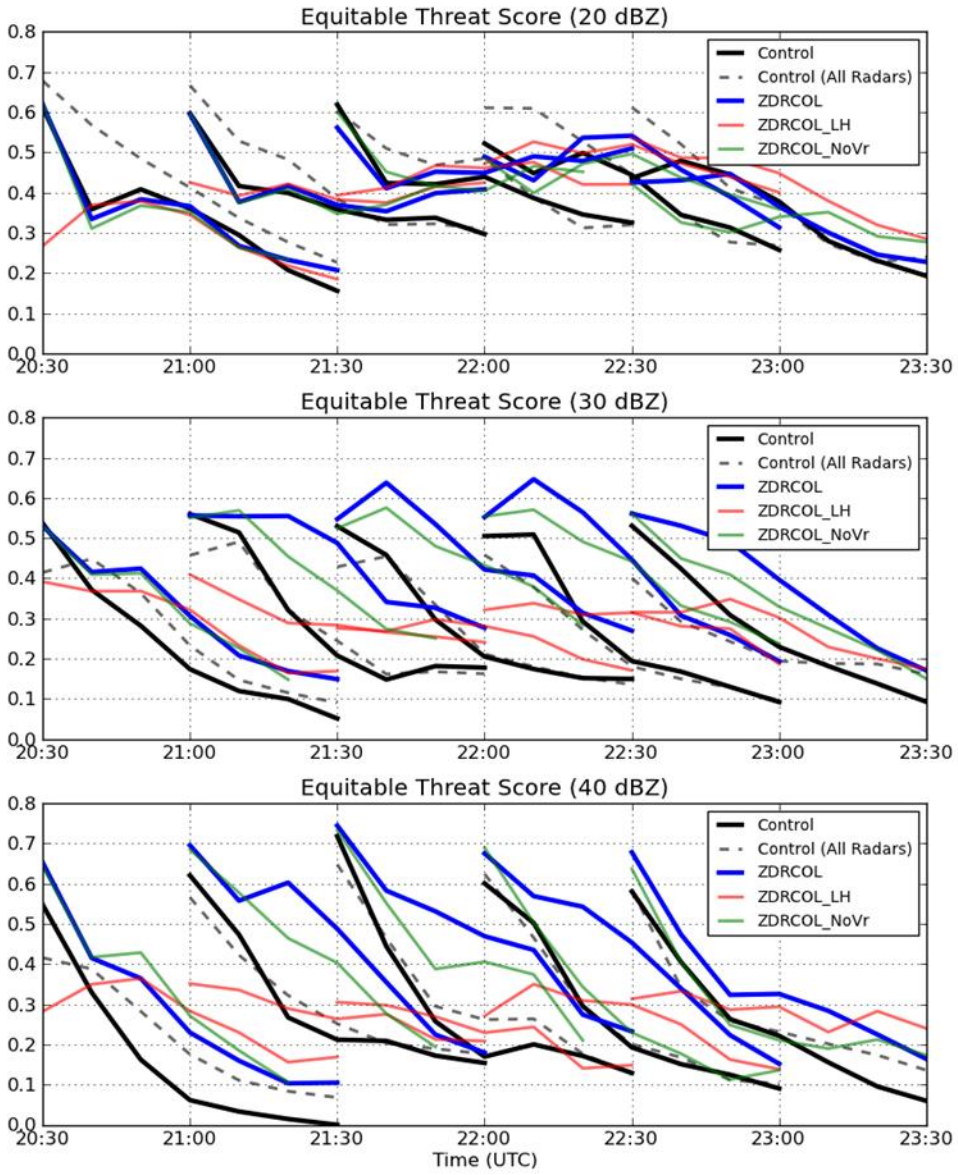

Fig. 9: Equitable threat score of each run for each 1-hr forecast for (top) 20-dBZ, (middle) 30-dBZ, and (bottom) 40-dBZ thresholds of composite reflectivity.